Investigation of Abundance Planes to Isolate Accreted Stars

Elise Tellander

Division of Astrophysics
Department of Physics

Lund University

2026–EXA263

Degree project of 15 higher education credits
June 2026

Supervisors: Thomas Bensby & Joshua Povick

Division of Astrophysics
Department of Physics
Box 118
SE-221 00 Lund
Sweden

Abstract

The formation of our Galaxy has long been a rewarding area of research within astronomy. A large part of analysis includes using kinematics to separate the different structures in the Milky Way and also to discover accreted stars. While it is highly useful to understand the motions of populations there are systematic errors that follow, due to the difficulties of getting high quality data for them. There is also the issue of stars having their kinematics perturbed due to interactions with other objects. Abundances do not have those problems, as stars retain the chemistry of the gas cloud they formed out of. This makes them excellent tracers for events concerning the formation of the Milky Way, since the chemical makeup will act as a fingerprint, revealing where it formed and if it originates from another galaxy. The aim of this project is to evaluate different combinations of abundance planes in order to examine whether there exist additional ways to identify and isolate accreted stars. By using abundance data from APOGEE DR19, regions associated with accreted stars were isolated in the [Fe/H]-[Mg/Fe] and [Al/Fe]-[Mg/Mn] planes, where the stars were further divided into velocity groups. These velocity ranges represent the structures of the Milky Way, thus they can give an indication to whether a potential accreted population has settled into a certain region of the Galaxy. Considering the processes of chemical evolution in stars, the abundance planes of [Fe/H]-[Nd/Ce], [Nd/Si]-[Ti/Mn], [Ce/Mg]-[Mg/Fe], [Nd/C]-[Mn/Fe], [Nd/H]-[Mg/Mn] and [Co/Si]-[Ce/Mn] were investigated. The sample of stars were then plotted in these planes and observed how they moved depending on the abundances. Additionally some other groups were isolated in the hopes of observing clear trends across the planes. Two distinct regions were observed, the first occupying $-1.5 <$ [Nd/Si] < -1, the second being able to be separated into three groups defined by group 1: $-0.5 <$ [Nd/Si] < -0.3 & [Ti/Mn]< 0, group 2: $-0.2 <$ [Nd/Si] < -0.1 & [Ti/Mn]< 0 and group 3: $0.05 <$ [Nd/Si] < 0.15 & [Ti/Mn]< 0.

The isolated stars display clear dependence on Nd, separating into distinct groups when an abundance plane includes Nd but appear to be clustered together when displayed in other abundance planes. While this analysis can not definitively say that these stars are relics from an accretion event, it has been shown that Nd can be a powerful element to use when further separation of an accreted population is needed.

Popular summary

It is in human nature to be curious, to wonder where we came from and what exists outside of our small corner of the Universe. While some people are content to just wonder, others take it upon themselves to try to find answers to the many mysteries surrounding us. The vastness of space invites research from various angles to increase our understanding the Universe. The formation of galaxies is one of the major mysteries that has puzzled astronomers for ages. But as human technology has become increasingly advanced, we are now able to study the Universe in even better detail. And to get a closer look at galaxies we only need to look at the space around us, as we are surrounded by our home Galaxy, the Milky Way. It is the host of numerous stars, planets and various other astronomical objects that can be used to investigate its formation history.

So how can we gain an understanding of something so big as a galaxy? Just like archaeologists use the remnants of civilisations past to piece together the history of the Earth, astronomers can use data collected from the various objects in space to unveil the history of the Universe. A major piece of the puzzle is the origin and evolution of the chemical elements. The processes which allow the elements to form and how they then are distributed across the Galaxy allow for a closer insight into how the Galaxy was formed and became what it is today.

Stars are born from regions of dust and gas, fusing together elements to sustain enough outgoing pressure to stave off a collapse. As these stars grow older and die, the elements produced during their lifetime—i.e. their chemical makeup—will be returned to the surroundings, and a new generation of stars can be born from the remnants. Different types of explosive endings release different elements, which can act as a special fingerprint defining where a star was born and how old it is. This fingerprint can be used to discover foreign stars, those not formed by the dust and gas composing the Milky Way, instead having been poached from other galaxies. These are called accreted stars, which were left behind following mergers between smaller galaxies and the Milky Way, during the tumultuous formation of our Galaxy. These stars will have the chemical makeup of their original galaxy, which is often distinct from the chemical fingerprint that defines the Milky Way.

Using the data collected from surveys of stars in the Galaxy we can look at the amount of each element contained in each star, also known as their abundances, and categorize them based on their properties. This is instrumental to understanding the formation history of the Milky Way, as this information combined with the star positions in the Galaxy will give valuable insight into the potential origin of the star. However, while there are certain well known abundances that will be more prevalent in accreted populations, they are still not enough to fully isolate the populations. Thus it is prudent to explore whether there exist other elements, or ratios of specific abundances, to figure out if there is a way to bring more certainty to the chemical analysis of accreted stars.

Contents

Chapter 1

Introduction

The formation of the Milky Way is one of the largest unknowns within astronomy, and while there has been huge progress in the past few years thanks to advancement in technology and quality of data, there is still not a conclusive explanation for the mechanisms behind the formation of galaxies. The leading theory is that the Milky Way is built up from the mergers of smaller galaxies based on data collected on stars and their kinematics, dynamics and chemical abundances (e.g Helmi, 2020, Kawata et al., 2026). However, there are not any definitive answers as to when this happened and what consequences it had on the Galactic structure as a whole. One way to understand the effects of galaxy formation is to examine the traces left behind from these events, such as accreted stars. Because the stars are made up of matter native to their birth galaxy, we can take spectroscopic data and potentially trace back their history to one specific event (Buder et al., 2024).

The majority of research involving galactic archaeology, i.e. the study of uncovering the history of galaxy formation, focus on the Galactic halo since there is clear evidence of multiple, previous merger events contained in it. This leads to the halo being an ideal structure to research in the advancement of galactic archaeology (Helmi, 2020). While studying the halo offers a clearer view of older stellar populations, it potentially leaves out information about past accretion events that shaped the inner regions of the Milky Way. In order to understand the mechanics behind galaxy formation it is important to take a deeper look into the Milky Way's many regions to discover how these different parts were created during the formation of the Galaxy. Especially considering that a large portion of the halo's density is contained in the centre of the Galaxy, making it more than likely that there could be a hidden population that would give additional insight into the formation (Matteucci et al., 2019).

The chemical distribution of stars is a key component for galactic archaeology, as it gives valuable insight into the merger history of the Milky Way. In understanding how it has interacted with other galaxies by looking at the traces left behind, we can shed light on potential formation events that have been instrumental for the current state of the Galaxy. One way of exploring this is by focusing on accreted stars, the ones left behind by merger events in contrast to stars formed in-situ. Accreted stars are primarily found in [Mg/Mn] versus [Al/Fe] plane, but their range of values is not exclusive to accreted stars and includes stars formed in-situ (Hawkins et al., 2015). Additionally, if the goal is to determine whether some stars belong to one specific merger event, it will be hard to separate them with just one plane (Buder et al., 2024). There has already been studies evaluating the usefulness of using different abundance ratios to separate accreted stars from the rest of the population. However, the majority of research is limited to the Galactic halo (Hawkins et al., 2015). While the halo is a crucial part of explaining the formation history of the Milky Way, exclusive focus on the properties of the halo's accreted population could cause a bias when applying those same properties to the stars in the other regions. With how many stars there are in the plane and towards the centre of the Milky Way there could be previously unidentified anomalies in the assumed in-situ population, leading to the need for a more involved method of defining the accreted stars.

It is thus imperative to find multiple ways to better isolate accreted stars, because while the kinematics of stars change on a relatively shorter time-scale, one can consider that the chemical composition will remain roughly constant for a single star over a cosmic time scale (Buder et al., 2021). Therefore, investigating how stars are positioned in various abundance planes and seeing if there is a trend in the abundance values for accreted stars would lead to a better understanding of how merger events have affected the formation of the Galaxy. Although researching the Galactic halo is important it should not be the sole focus of where to look for merger events, as there is very likely valuable information hidden in the Galactic plane and towards the centre of the Galaxy. Thus by using the information garnered from identifying accreted stars in different abundance planes we can get a better idea of what types of merger events has contributed to the formation of the Galaxy. In addition it will also make it easier to distinguish different merger events from each other, which leads to the possibility of tracing these abundances back to their galaxy of origin. Hence looking for accreted stars in various abundance planes and evaluating their significance will help broaden the definition of them, and applying this to the different Galactic regions will make it possible to identify merger events that could lead to an increased understanding of the Milky Way's formation.

In this thesis these questions will be addressed by investigating abundance planes concerning accreted stars, by using chemical abundance data and ratios between them to understand how stars migrate across the abundance planes created. A sample of potential accreted stars are created by using previously found selections (Nissen & Schuster 2010 and Hawkins et al. 2015). This sample is then projected onto the different planes, and groups that stand out are isolated and then examined if these groupings are preserved across different abundance planes. This is done in order to understand whether there exist some trends in the abundances of accreted stars which could make it easier to discover and isolate them from in-situ formed stars and other accreted populations.

Chapter 2

Theory

2.1 The Milky Way

There are three major structures that make up the Milky Way: the bulge, the disk, and the halo. The bulge is located in the central region of the Galaxy, the disk extending outwards into the plane, and the halo surrounding the Galaxy. In between the stars that make up the Galaxy there is the interstellar medium (ISM), comprised of dust and gas and primarily concentrated around the Galactic plane and towards the Galactic centre. This makes it harder to observe objects in these regions due to extinction, i.e. the ISM interfering with the light leading to a worse quality of the obtained data.

The chemical elements that make up a star can also be used for identification, where stars that have a high amount of atoms heavier than He are called metal-rich, while those with a low amount are called metal-poor (usually [Fe/H]< -0.8 dex). High amounts of Fe atoms signify a metal-rich star. The α-elements (those that can be produced by combining ^{4}He atoms, such as O, Mg, Si, S, Ca and Ti) are also commonly used as an indicator for populations, where the α-rich stars are also usually metal-poor.

Helmi (2020) writes that the Galactic halo extends far from the Galactic plane and is host to some of the oldest and most metal-poor stars with [Fe/H]< -0.8 dex. It is not densely populated and the majority of the mass density is situated at the centre of the Galaxy with distinct high velocities of $V_{\mathrm{tot}} > 200$ km s^{-1}. Further divisions in the structure can be made, because there is evidence of accreted structures that have settled into the halo, likely the last major merger experienced by the Milky Way.

The disk of the Milky Way can be separated into two prominent structures, the thin disk and the thick disk. This is commonly done with the chemical abundance of stars, specifically the ratio of α-elements to Fe ([α/Fe]). That leads to a clear distinction into a group with high-[α/Fe] and one with low-[α/Fe], defined as the thick and thin disk respectively. The thin disk has ongoing star formation that appears to have started ~ 8 Gyr ago, with stars generally having a lower total velocity and a metallicity above [Fe/H] $\gtrsim -0.8$ (Hawkins et al., 2015).

Defining the populations by velocity should be done with caution as there is often overlap between populations, due to processes that can kinematically cool and heat stars. Thin disk stars have velocities of $V_{\rm tot} \lesssim 50$ km s^{-1}, while thick disk stars can be considered to have velocities in the range 70 km s^{-1} $< V_{\rm tot} <$ 180 km s^{-1} (Bensby et al., 2014). However, there are high-α stars with velocities in the range $180 < V_{\rm tot} < 210$ km s^{-1} that could belong to a heated thick disk (Nissen & Schuster, 2010).

The Galactic bulge seems to be an intersection of all regions, where both the halo and the thin and thick disk seem to intermix within the region, while still having its own population associated with it (Bensby et al., 2017). Observation of the bulge is problematic due to the large of extinction associated with the plane and the Galactic centre, making it difficult to get reliable data for this region. In a review of the bulge by Zoccali & Valenti (2026) it is stated that there seems to be two populations present, one metal-rich and one metal-poor, with stars being found in a broad metallicity range $-1.5 \leq$ [Fe/H] $\leq +0.5$ dex. These populations seemingly belong to two components with different morphologies, as the metal-rich stars follow a boxy/bar orbit while the metal-poor stars are confined to a spheroid shape, which could be the result of some formation pathway. The metal-poor stars also display a similar trend in [α/Fe] as seen in the thick disk, additionally this component is older at around 10 Gyr. On the contrary, the metal-rich stars are of younger ages, which could mean that there were multiple star formation epochs in the bulge. However, this is still debated as there is conflicting data, and could be the result of thin disk stars being mistakenly though of as bulge stars, or the selection effects creating differences.

2.2 Origin of the elements

The abundance of a star is defined as the number density of a specific atomic species, including all its ionized states, compared to the number density of hydrogen atoms. The abundance is commonly used when investigating the chemical properties of a star, with the Sun used as a baseline. The widely used bracket notation for abundance ratios is defined as

$$[\mathrm{X/Y}] = \log_{10}\left(\frac{N_{\mathrm{X}}}{N_{\mathrm{Y}}}\right) - \log_{10}\left(\frac{N_{\mathrm{X}}}{N_{\mathrm{Y}}}\right)_{\odot}, \qquad \text{(Eq. 2.2.1)}$$

where X and Y are arbitrary chemical species for the star and $\mathrm{X}_{\odot}$, $\mathrm{Y}_{\odot}$ are the same ones but for the Sun. N represents the number density of the specific atomic species. The square brackets mean relative to the Sun on a logarithmic scale (Gray, 2005). The metallicity "M" of a star is defined as the total abundance of elements heavier than He and is sometimes used in the ratio calculation, but it is close enough to the value of [Fe/H] that it is often used to refer to metallicity instead (Mészáros et al., 2025), which will be utilized in this work.

Since the chemical elements are created in different nucleosynthetic processes at different stages of life, the ratio of two abundances can give information on its stage of evolution and its birth region in the Galaxy. To gain an even deeper understanding of the properties of stars one can use abundance planes, which are made by plotting two abundance ratios against each other. By investigating the location of stars on these graphs we can infer which structure and population a star belongs to, based on the information available (e.g. Hawkins et al. 2015).

The nucleosynthetic processes of chemical evolution in stars and the following enrichment of the Galaxy is thoroughly described in Kobayashi (2026) and references therein. Here, the relevant information is summarized in the following paragraphs, with some additional material.

When a star reaches a core temperature of 10^7 K it can start fusing hydrogen into helium. After the H in the core is used up and becomes an inert He core, H burning will ignite in a thin shell outside the core, which will continue outwards until the core is hot enough to start fusing He into C. Following that, He burning can start in a layer surrounding the core pushing the star into the Asymptotic Giant Branch (AGB) phase. This burning is unstable which leads to the mixing of the core and envelope, enabling a larger yield of lighter elements such as C, N and F. When the core becomes inert due to the build up of C and O, a lower mass star will stop fusion in its core because the temperature is not sufficient to continue burning, which leads to it expelling its envelope and then cooling into a white dwarf (WD). As for more massive stars, the fusion process continues on to produce heavier elements. The more mass a star has, the higher its yield of the α-elements (e.g., O, Ne, Mg, Si, S, Ar, Ca) will be. There is also the production of odd-Z elements (e.g., Na, Al, P, Cu) whose formation is dependent on the amount of free neutrons available. This is important for galactic archaeology, since stars born from remnants with a higher metallicity will have access to more neutrons, leading to a larger yield of odd-Z elements. When the nucleosynthesis has reached Fe there is no longer enough radiative energy to sustain the star and it collapses. The elements produced in the star are released into the surroundings by following supernovae (SNe). During this brief time, nucleosynthesis is initiated in the matter ejected from core-collapse supernovae (CCSNe) due to the enormous pressure. This produces the elements around Fe, called Fe-peak elements, which include Cr, Mn, Zn and Co. The yield of Fe-peak elements depend on the completion of the Si burning, because Cr and Mn are produced in the regime of incomplete Si burning and Zn and Co are created in the complete regime.

Type Ia supernovae (SNe Ia) involve WDs, where a WD is either accreting enough material from a companion star to explode (single-degenerate), or it merges with another WD. In this type of SNe it is expected to produce a majority of Fe, but models mentioned in the article find that the Fe-peak elements Cr, Mn and Ni are also a larger part of the output, SNe Ia being responsible for a large portion of the synthesis. The same model also shows that for WDs with lower masses, SNe Ia is responsible for some of the production of Si, S, Ar and Ca, which are most commonly associated with CCSNe.

Atoms heavier than Fe, like Ce and Nd, are formed by neutron-capture processes. In the slow neutron-capture process (s-process), these elements can be produced when there are free neutrons available. This enables the production of heavier elements even in smaller-mass stars. The enrichment of s-process elements is considered to be primarily from AGB stars due to their neutron densities. The rapid neutron-capture process (r-process) occurs in explosive events where there is an abundance of free neutrons, enabling the rapid formation of elements. The sites for this process are thought to be both neutron star mergers and CCSNe, although the main enrichment site is still debated. In Kobayashi et al. (2020) it is stated that the abundance of s-process elements are expected to be lower in regions that experienced accelerated star formation due to the long time it takes for AGB stars to enrich its environment. As for the amount of Ce and Nd produced by the two processes, Das et al. (2020) attributes 90% of Ce to the s-process, while Battistini & Bensby (2016) states that the s-process is responsible for 56% of the Nd production.

2.3 Galactic archaeology

With all the information contained in stars they are a prime source for understanding the past of our Galaxy. The different production rates and mechanisms have obvious consequences observed in the stellar atmosphere. The abundance of a star is dependent on the gas it formed out of, and it is expected that this chemical signature will be well preserved. On the contrary, kinematics and orbits can change over time due to interactions in the Galaxy, which makes abundances ideal for investigating the history of the Galaxy (Helmi, 2020). Mergers play a major role in the formation of the Milky Way, from providing material for star formation to disrupting orbits, and have affected the way the Galactic structure culminated in what we see today. This is why it is important to find ways to identify the signs of a merger, specifically by using the chemistry of stars. Hawkins et al. (2015) sought to find additional ways to distinguish the Galactic disk and halo by only using the chemical abundances as velocity is not a perfect separator of populations. They found that the abundance planes [α/Fe], [C+N/Fe], [Al/Fe] and [Mg/Mn] were able to distinguish the different regions efficiently, while some abundances showed no clear trend for the different structures. Their analysis also showed that the in-situ halo and thick disk are not so distinct in abundance planes, with the thick disk often extending to lower metallicities and into the regions of where the halo is thought to be displayed. In addition, they found stars that belonged to the thin disk that had metallicities below [Fe/H]< -0.8. However, chemistry cannot only be used to separate Milky Way structures, but also to potentially identify accreted structures. For example, Nissen & Schuster (2010) found evidence of two distinct populations of halo stars, differentiated by their respective abundances of the α-elements. They report a clear distinction in the [Fe/H]-[Mg/Fe] abundance plane, where they suggest that the low-α stars could be of accreted origin. Upon further research, these stars seem to belong to a previous merger event that became known as the Gaia-Encleaus/Sausage (GES) (Helmi, 2020), that happened 8-10 Gyr ago and was likely the last major merger that the Milky Way experienced (Kawata et al., 2026). Das et al. (2020) observed a population of stars that also appear to be in line with the GES merger, with metallicities that range from -2.5 to -0.5 and ages that span 8 to 13 Gyr.

As for studies looking for accreted streams in the MW disk, a study conducted by Feuillet et al. (2022) found that there appeared to be a distinct population of accreted stars, with velocities indicating that the population was confined to the stellar disk (rotational velocity $V_{\rm rot} > 110$ km s^{-1}). This population also had [Al/Fe] < -0.2, but contrary to the known accreted halo population the values for [Mg/Mn] were lower, strengthening the conclusion that this originates from a separate merger event than the ones building up the halo, that could have happened about 2×10^9 years ago. Necib et al. (2020) observed a stream of likely accreted stars in the solar neighbourhood that displayed a strong coherence in velocities. A small part of their sample had associated abundances, which showed an average value of -0.55 for [Fe/H] and 0.13 for [Mg/Fe]. In regards to the bulge, Horta et al. (2021) suggest a significant merger which deposited metal-poor stars within $R \sim 4$ kpc of the bulge. The stars from this event have low abundances of Al, C, N and Ni and are chemically distinct from other identified accreted structures. This structure has an estimated mass of 5×10^8 $M_\odot$, and likely interacted with the MW in its early history before any major structures, like the bulge, formed.

Chapter 3

Data and Method

3.1 Spectroscopic data

The spectroscopic data comes from the Apache Point Observatory Galactic Evolution Experiment H-band spectrograph (APOGEE; Majewski et al. 2017) as part of SDSS V's data release 19 (hereafter DR19 Kollmeier et al. 2026). The data was collected by 2.5-m Sloan Digital Sky Survey telescope (SDSS) at Apache Point Observatory (Gunn et al., 2006) and the 2.5-m DuPont telescope at Las Campanas Observatory (Bowen & Vaughan, 1973) using a high resolution multi-fibre spectrograph APOGEE (Wilson et al., 2019). The abundance data was processed using the ASPCAP abundance pipeline (García Pérez et al., 2016) and the distances were then supplemented with the StarHorse catalogue (Queiroz et al. 2020, 2023) adapted for DR19 giant stars (SDSS Collaboration et al., 2025). StarHorse is a Bayesian tool that derives stellar parameters from astrometric, spectroscopic and photometric data, which can improve the precision for parameters such as distances, extinction and temperature.

To ensure the quality of the data stars that had FLAG_BAD toggled were removed. In addition to that flag, all elements have flags associated with them to signify the quality of the data. All stars that had dubious data flagged by either FLAG_BAD or the specific abundance flags were removed from the set. If the program flag OPEN_FIBRE was set the star was also excluded, to not include biases that would be introduced from specific targeting. In addition to removing certain flags, the dataset was also confined to the following ranges to ensure the quality, based on the limits written in Mészáros et al. (2025).

- $3500\ \mathrm{K} < T_{\mathrm{eff}} < 6000\ \mathrm{K}$
- $0 < \log g < 3.8$ dex
- $\varpi > 0$ mas
- $\mathrm{S/N} > 100$
- $[\mathrm{M/H}] > -2.4$
- $d/\sigma_d > 5$,

Where ϖ is the parallax, d is the distance and σ_d is the distance error. These restrictions led to a parent sample of 81768 stars. Additionally, Mészáros et al. (2025) details a correction for the abundance data based on the effective temperature and provides the correction coefficients. The zero-point offsets for the different abundances are calculated as $\Delta[\mathrm{X/M}] = a \cdot T_{\mathrm{eff}} + b$, where a, b are the correction coefficients mentioned above. Thus the correction was calculated as

$$[\mathrm{X/H}]_{\mathrm{corrected}} = ([\mathrm{X/H}]_{\mathrm{calib}} - [\mathrm{M/H}]) - \Delta[\mathrm{X/M}] + [\mathrm{M/H}], \qquad \text{(Eq. 3.1.1)}$$

for each element available. $[\mathrm{X/H}]_{\mathrm{calib}}$ is the internally calibrated abundance data. Due to the APOGEE abundance data being in the form of [X/H], while the correction is done using the metallicity ratio [X/M], the values had to be converted twice in that order to get the final result of $[\mathrm{X/H}]_{\mathrm{corrected}}$ since the ratios are logarithmic. The abundances for P, V and Cu were described as poor quality and did not have a correction, thus they were not included in this project.

The positional information was transformed into a galactocentric frame with Astropy (Astropy Collaboration et al., 2022). The solar values used for the transformation were $(U_\odot, V_\odot, W_\odot) = (9.65, 14, 8.57)$ km s^{-1}, $R_\odot = 8.275$ kpc and $z_\odot = 20.8$ pc, provided in Kawata et al. (2026).

3.2 Selection of potentially accreted stars

The selection of the sample was motivated by Hawkins et al. (2015) exhibiting that accreted populations can be found in specific regions with low [Mg/Fe] and [Al/Fe]. The sample of potentially accreted stars is initially separated by linear functions determined by eye in both the [Fe/H]-[Mg/Fe] plane and the [Al/Fe]-[Mg/Mn] plane, seen in Fig. 3.1. The accreted population is defined as stars existing below the line in the [Fe/H]-[Mg/Fe] plane and to the left of the line in the [Al/Fe]-[Mg/Mn]. With these additional restrictions the final sample size is 1472 stars.

The stars were then divided into five groups based on kinematics, with the velocity ranges chosen to represent typical values for the different compartments of the Milky Way (see Section 2.1). The low velocity group is defined by $V_{\mathrm{tot}} < 70$ km s^{-1}, primarily associated with thin disk stars. The ranges $70 < V_{\mathrm{tot}} < 110$ km s^{-1} and $110 < V_{\mathrm{tot}} < 180$ km s^{-1} encompass the thick disk star velocities. This group was split into two ranges to be able to compare the sample to the results of Feuillet et al. (2022), who found an accreted population in the disk with $V_{\mathrm{tot}} < 110$ km s^{-1}. $180 < V_{\mathrm{tot}} < 250$ km s^{-1} may include some heated thick disk stars, but is mainly halo stars. Stars with velocities following $V_{\mathrm{tot}} > 250$ km s^{-1} belong to the halo.

These divisions are included to understand the kinematics of the sample, since the dynamics of merger events can lead to stars ending up on orbits with velocities comparable to those of the different structures. So stars with low velocities could have been captured by the disks of the Milky Way as described in Feuillet et al. (2022), while stars with high velocities could belong to the halo, or they have been heated to higher velocities.

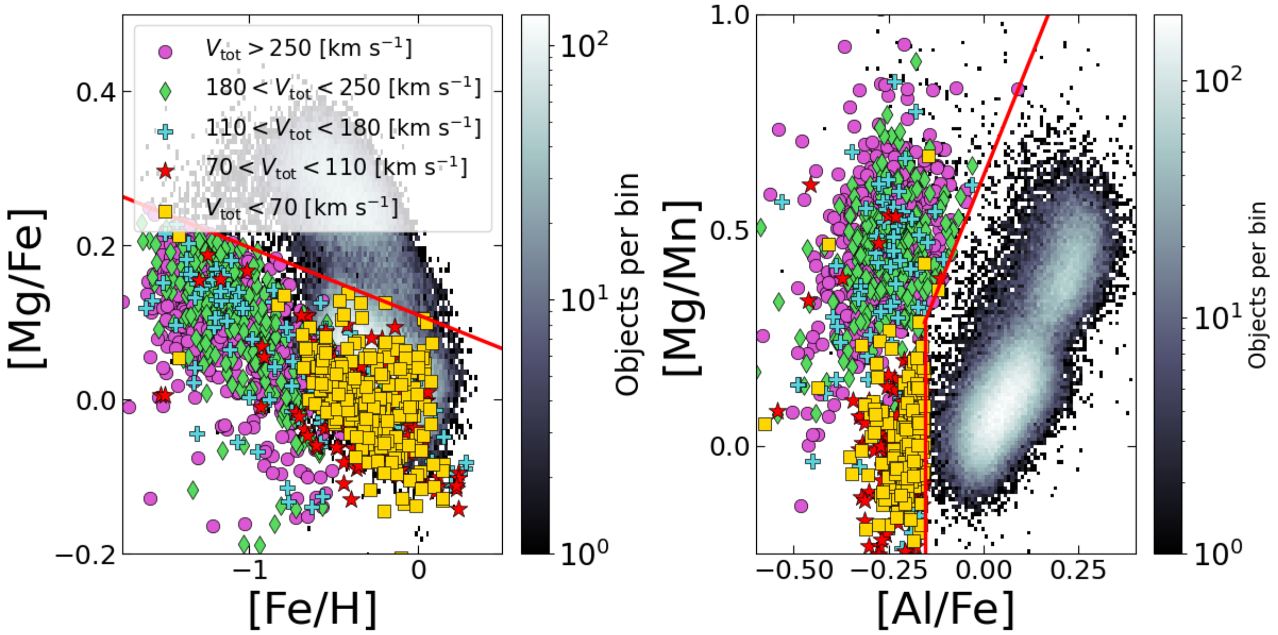

Figure 3.1: The selection of the sample was done by isolating regions in the [Fe/H]-[Mg/Fe] and [Al/Fe]-[Mg/Mn] abundance planes. The scattered points are divided into velocity ranges to make it easier to identify potential groups. The purple circles denote stars with $V_{\rm tot} > 250$ km s^{-1}, green diamonds for $180 < V_{\rm tot} < 250$ km s^{-1}, blue plusses for $110 < V_{\rm tot} < 180$ km s^{-1}, red stars for $70 < V_{\rm tot} < 110$ km s^{-1}, and yellow squares for $V_{\rm tot} < 70$ km s^{-1}.

The components of the Milky Way were defined as well to compare with the separated stars. They are presented in Table. 3.1. Since the bulge is said to be the intersection of multiple

Table 3.1: The properties used to define the Milky Way structures for comparison, the source of the values is written in Section 2.1. Line refers to the respective cuts made to the planes seen in Fig. 3.1.

	Velocity	[Fe/H]	[Mg/Fe]	[Mg/Mn]
Halo	$V_{\rm tot} > 200$ km s^{-1}	< -0.8 dex	Above line	None
Thick Disk	$70 < V_{\rm tot} < 180$ km s^{-1}	None	Above line	Below line
Thin Disk	$V_{\rm tot} < 50$ km s^{-1}	> -0.8 dex	Below line	Below line

populations, as well as less data being available close to the Galactic centre, there is no defined set of bulge-stars. They will instead be considered as in smaller values of distance from the Galactic centre R.

3.3 Abundance planes

The logic behind the [Al/Fe]-[Mg/Mn] plane is to compare the rate of production of the odd-Z elements (e.g. Al), and the α-elements (e.g. Mg), in comparison to the Fe-peak elements (e.g. Fe, Mn). The abundances of different elements will depend on a galaxy's star formation rate. So for a galaxy like the Milky Way with a fast star formation rate there will be a higher abundance of α-elements at low metallicities, that will successively decrease as SNe Ia start to enrich the environment with Fe-peak elements. Increased amounts of free neutrons

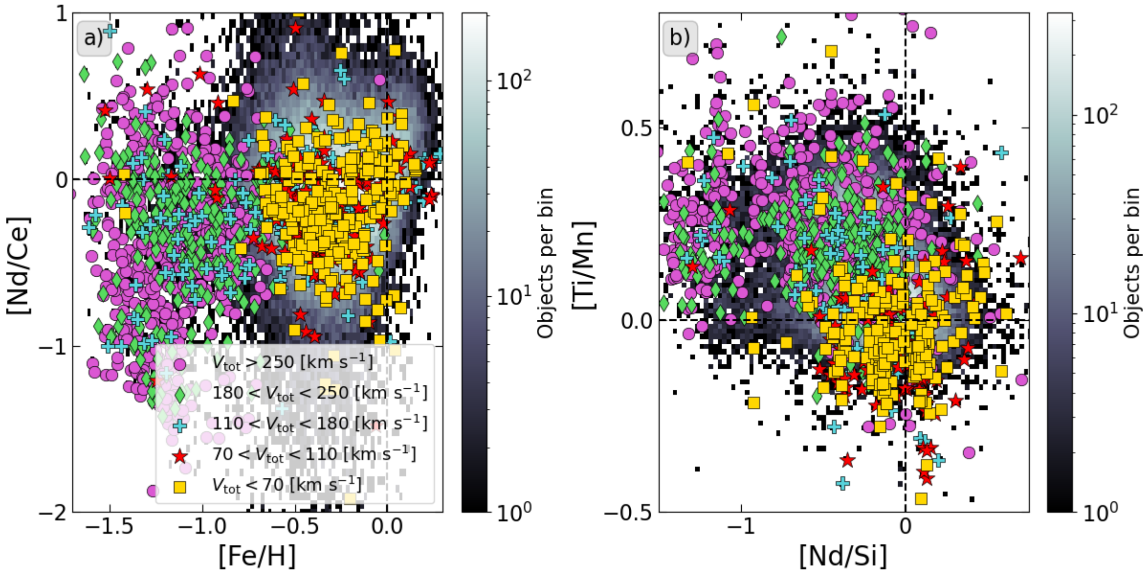

Figure 3.2: Four of the chosen abundance ratios and two of the planes they can create. The scattered points are the same as in Fig. 3.1

also become available, affecting the abundances of the odd-Z elements. The ratios of [Al/Fe] and [Mg/Mn] are thus ideal to determine the evolution mechanisms that are attributed to the different populations. This reasoning was reproduced when configuring other abundance planes, where the abundance ratios were considered based on how the element is produced and if its production could be affected by another element. The different production mechanisms of the elements are summarized in Section 2.2, and with that knowledge other abundance ratios can be produced to understand where a star was born and how it has evolved during its lifetime. The neutron-capture elements may be of particular interest, as they have so far not been readily used in either of the well established abundance planes used to discover accreted stars. They could then potentially be used to further separate the accreted stars, since the abundance of neutron-capture elements is dependent on the previous enrichment of the environment. The neutron-capture elements available in DR19 are Nd and Ce, where Nd can signal both r- and s-process production and Ce primarily indicates s-process production. Since the plane [Al/Fe]-[Mg/Mn] includes the three other major elemental groups (odd-Z, Fe-peak and α-elements), creating more planes with exclusively these processes did not display any interesting patterns. The Nd ratios are [Nd/C], [Nd/Si], [Nd/Ce] and [Nd/H] while the ones for Ce are [Ce/Mg] and [Ce/Mn]. [Co/Si] could potentially be interesting as the production of Co is dependent on the amount of Si present in the star at the time of the collapse. So a higher value of the ratio could indicate the star being formed an environment where the previous generation could reach a larger completeness regime for Si-burning. The ratio of [Mn/Fe] represents the ratio of SNe Ia and CCSNe that could indicate the enrichment history of the gas a star was born in. Finally [Ti/Mn] is considered because the production of Ti does not depend on progenitor metallicity, but Mn will increase as SNe Ia initiates, which could create a visible trend and additionally indicate the age of the stars. Two of the investigated abundance planes can be seen in Fig. 3.2, with the sample group displayed in each plane.

Chapter 4

Results

4.1 Isolated groups

Any groups that stood out, with either similar kinematics being grouped in a certain region or had abundance ratios towards the extreme ends, were isolated and plotted in multiple planes to see whether the groups were preserved or would scatter. In Fig. 3.2 b) there are four groups that stand out due to an increased density of points, which have been circled in the [Nd/Si]-[Ti/Mn] plane in Fig. 4.1. These groups are of particular interest since stars with similar origins are likely to occupy the same regions in abundance space, which could mean that these stars formed together. That is why it is interesting to see if these groups stay together in other planes, since it would strengthen the idea that these groups have the same origin.

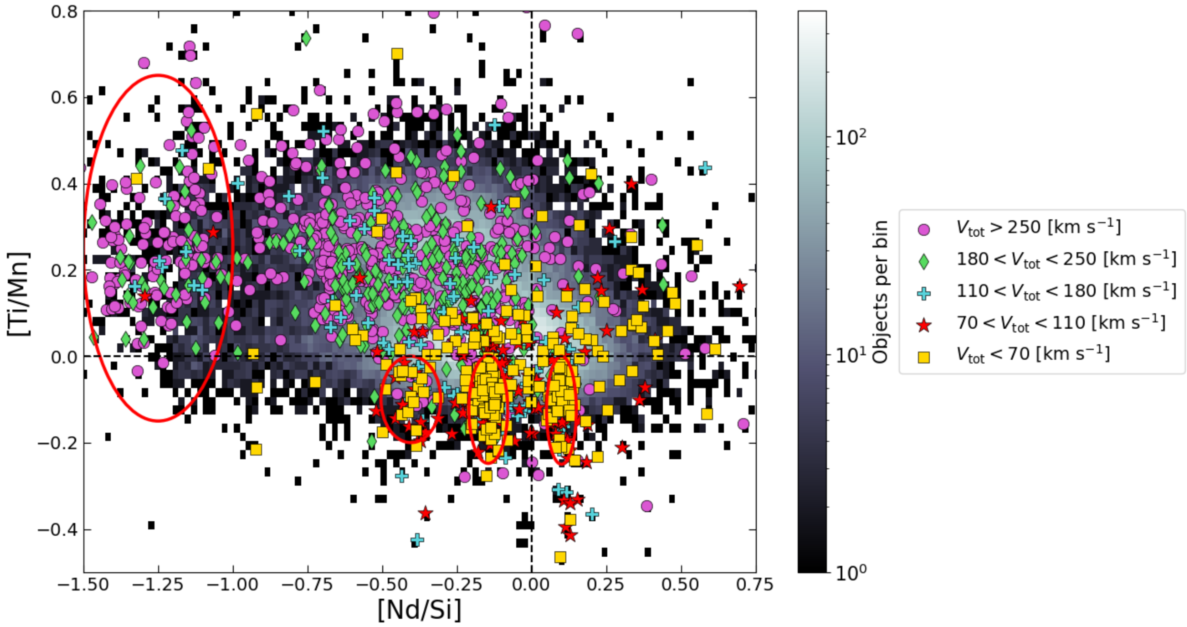

Figure 4.1: The [Nd/Si]-[Ti/Mn] plane seen in Fig. 3.2 b), where the red circles highlight the referenced groups of interest. The dashed line indicate the solar abundance.

The first isolated region of stars has a noticeably lower [Nd/Si] ratio, hereby known as the low-[Nd/Si] group, with [Nd/Si]< -1. The group is in the same range of [Ti/Mn] as the rest of the sample with high velocities. The other groups are primarily stars with disk-like kinematics and a low-[Ti/Mn] ratio, but appear to have differences in the Nd abundances since there are three distinct clusters as highlighted in Fig. 4.1. These groups are as follows:

- Group 1: $-0.5 <$ [Nd/Si] < -0.3 & [Ti/Mn] < 0
- Group 2: $-0.2 <$ [Nd/Si] < -0.1 & [Ti/Mn] < 0
- Group 3: $0.05 <$ [Nd/Si] < 0.15 & [Ti/Mn] < 0.

The velocities, with respect to the local standard of rest (LSR), of these groups are plotted in a Toomre diagram in Fig. 4.2. It shows that the majority of the low-[Nd/Si] sample have velocities of $V_{\mathrm{tot}} > 250$ km s^{-1}, with some in the range $180 < V_{\mathrm{tot}} < 250$ km s^{-1}. As for the other three groups, they have primarily $V_{\mathrm{tot}} < 110$ km s^{-1}, with some higher total velocities. The position of the different isolated groups as a function of Galactic radius (R) and distance from the Galactic plane (z) in [Nd/Si]-[Ti/Mn] space can be seen in Fig. A.1. The low-[Nd/Si] group begins at the centre of the Galaxy and is spread out surrounding the plane, revealing no pattern to indicate a region of the Galaxy this group could be bound to. As for the low-[Ti/Mn] groups, group 2 and 3 are present within $R < 6.0$ kpc, while group 1 appears when $R > 6.0$ kpc, although they are all present within $|z| < 2$ kpc of the Galactic plane except for a few points.

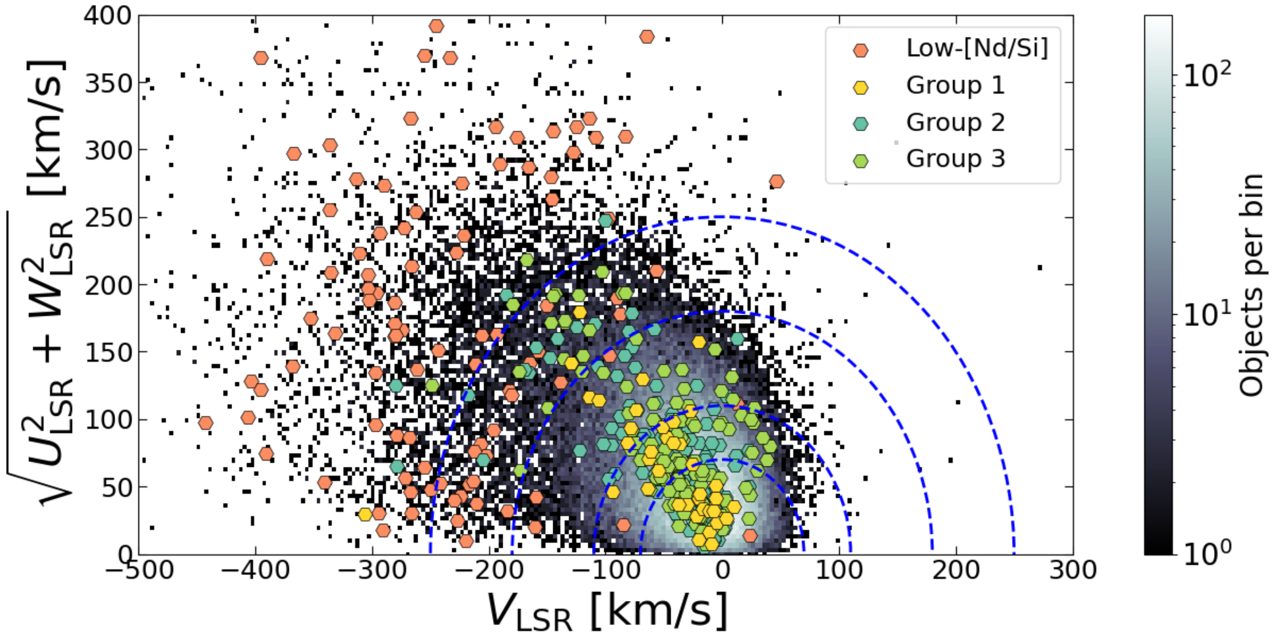

Figure 4.2: The isolated groups plotted in a Toomre diagram. The area between the blue dashed lines signify the five velocity ranges defined by V_{tot}.

Both isolated groups are plotted together in the different abundance planes together with the full sample coloured in grey. Fig. 4.3 display the [Al/Fe]-[Mg/Mn] and [Fe/H]-[Mg/Fe] planes. These planes show no separation for the three low-[Ti/Mn] groups, although they are situated in a narrow range for [Al/Fe]. There appears to be a denser region of points for the low-[Nd/Si] group with some stars scattered around it in both abundance planes.

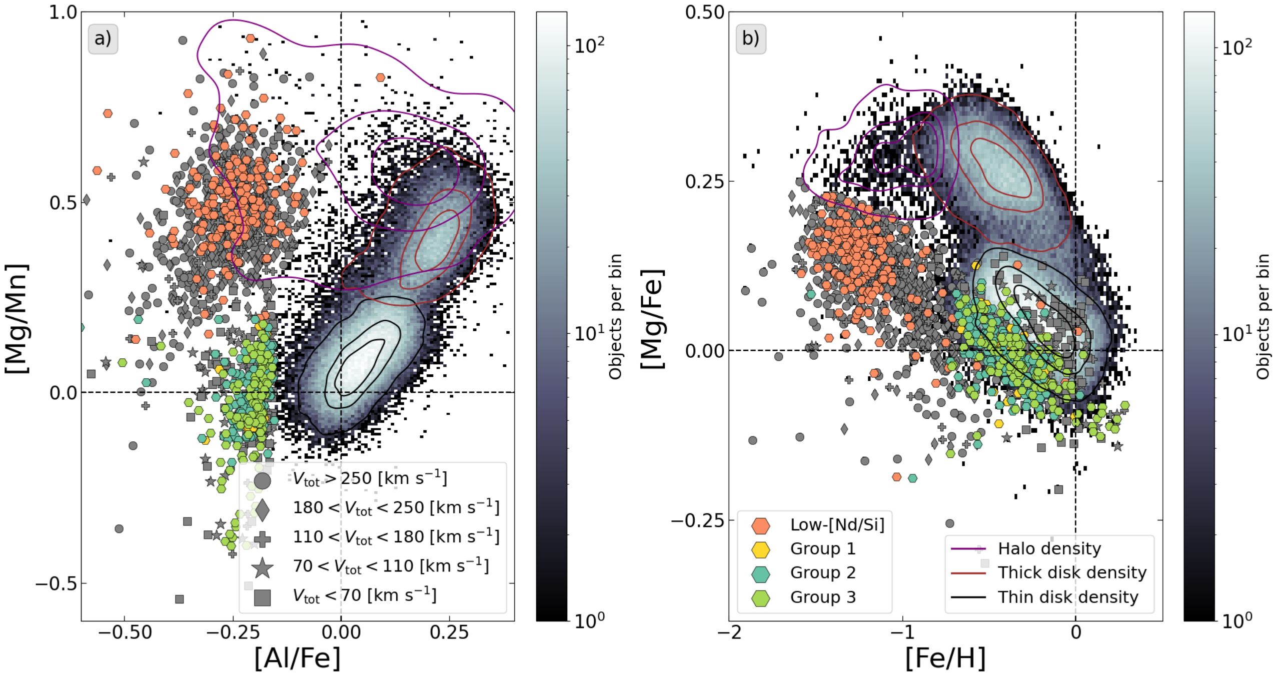

Figure 4.3: The four isolated groups plotted in the sample-defining abundance planes [Al/Fe]-[Mg/Mn] and [Fe/H]-[Mg/Fe]. The orange dots represent the low-[Nd/Si] region, the yellow dots represent the first low-[Ti/Mn] group with lower [Nd/Si] values, the blue dots represent the mid-range group and the green dots represent the high-[Nd/Si] stars. The grey points depict the rest of the sample, with the shapes representing each velocity range. The density contours represent the canonical halo (purple), thin (black) and thick (brown) disks defined by 3.1. The legends applies to both figures. The dashed line indicate the solar abundance.

Fig. 4.4 shows the planes [Fe/H]-[Nd/Ce] in a) and [Nd/Si]-[Ti/Mn] in b). The low-[Nd/Si] group display a much lower [Nd/Ce] abundance in the [Fe/H]-[Nd/Ce] plane compared to the rest of the high-velocity sample, while the metallicity range is the same. The low-[Ti/Mn] groups can be distinguished in this plane, although they are not cleanly separated. Group 3 has a larger [Nd/Ce] abundance than group 1 and 2, with group 1 having the lowest [Nd/Ce] of the three. The groups have the same range of metallicity. As for the [Nd/Si]-[Ti/Mn] plane, the low-[Nd/Si] group has values of [Ti/Mn]>0 except for a few points. The low-[Mn/Ti] groups are clearly separated in three distinct ranges of values in [Nd/Si].

In Fig. 4.5 the planes are [Nd/H]-[Mg/Mn] in a) and [Co/Si]-[Ce/Mn] in b). The low-[Nd/Si] group has very low [Nd/H] values but has halo-range values for its [Mg/Mn] ratio. The three low-[Ti/Mn] groups are separated with some intermixing in [Nd/H] and has a range of [Mg/Mn] both below and above solar values. Group 3 extends to much lower values of [Mg/Mn] than any other group. As for [Co/Si]-[Ce/Mn], the low-[Nd/Si] group has above solar values for [Ce/Mn] while a broad range in [Co/Si] like the rest of the high velocity sample. The three other groups do not appear distinct in this plane, with abundances that are aligned with the thin disk.

Fig. 4.6 display the planes [Ce/Mg]-[Mg/Fe] in a) and [Nd/C]-[Mn/Fe] in b). The low-[Nd/Si]

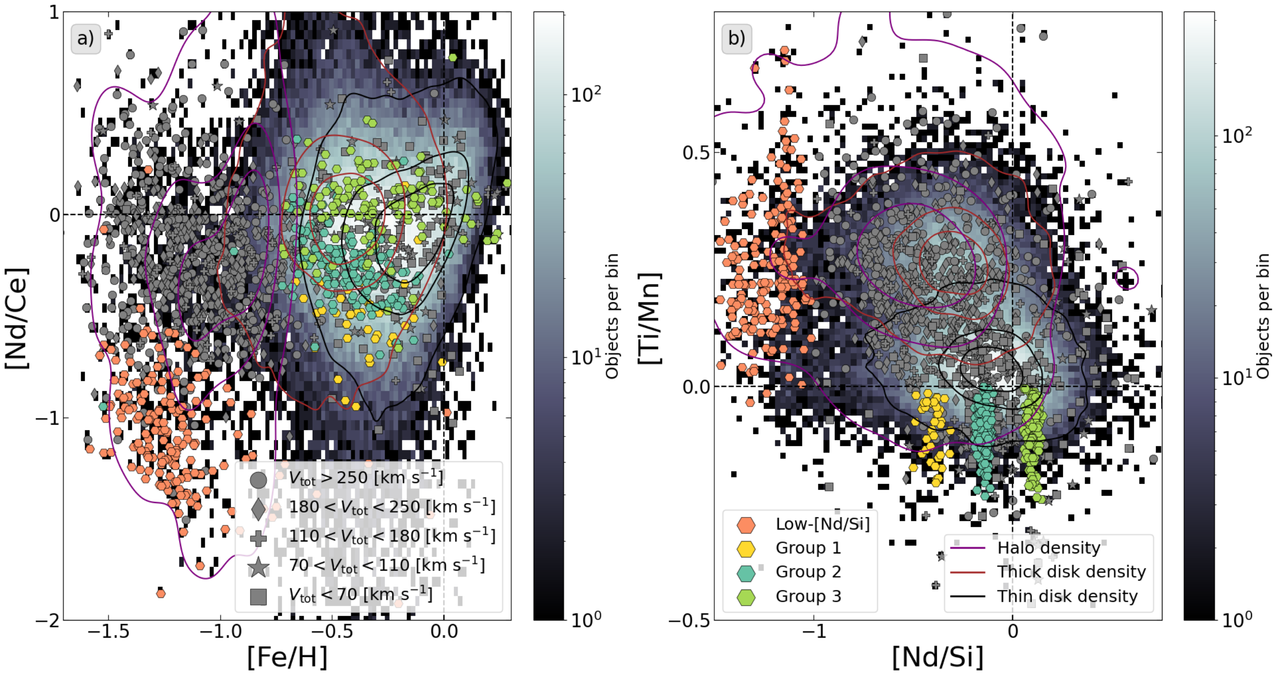

Figure 4.4: The same data as in Fig. 4.3, but in the abundances planes a) [Fe/H]-[Nd/Ce], and b) [Nd/Si]-[Ti/Mn]. The legends applies to both figures. The dashed line indicate the solar abundance.

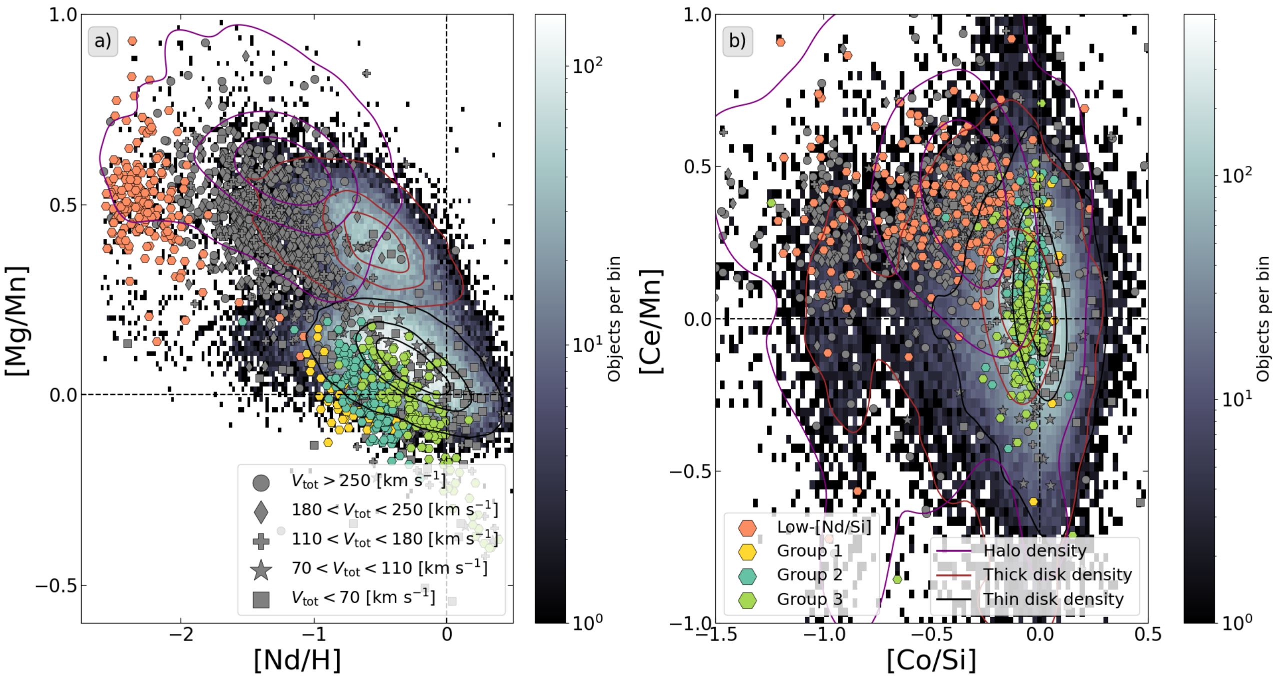

Figure 4.5: The same data as in Fig. 4.3 in the planes a) [Nd/H]-[Mg/Mn], and b) [Co/Si]-[Ce/Mn]. The legends applies to both figures. The dashed line indicate the solar abundance. The dashed line indicate the solar abundance.

and low-[Ti/Mn] groups have some minor intermixing above solar abundance for [Mg/Fe]. The value range for [Ce/Mg] appear to be similar for all groups, although the low-[Ti/Mn] have more points with [Ce/Mg]> 0. In the [Nd/C]-[Mn/Fe] plane the low-[Nd/Si] group has [Nd/C]< -1 and [Mn/Fe]< 0. The low-[Ti/Mn] groups are well separated by [Nd/C] with minimal overlap. The [Mn/Fe] ratio lies around the solar abundance, although group 3 reaches higher values of

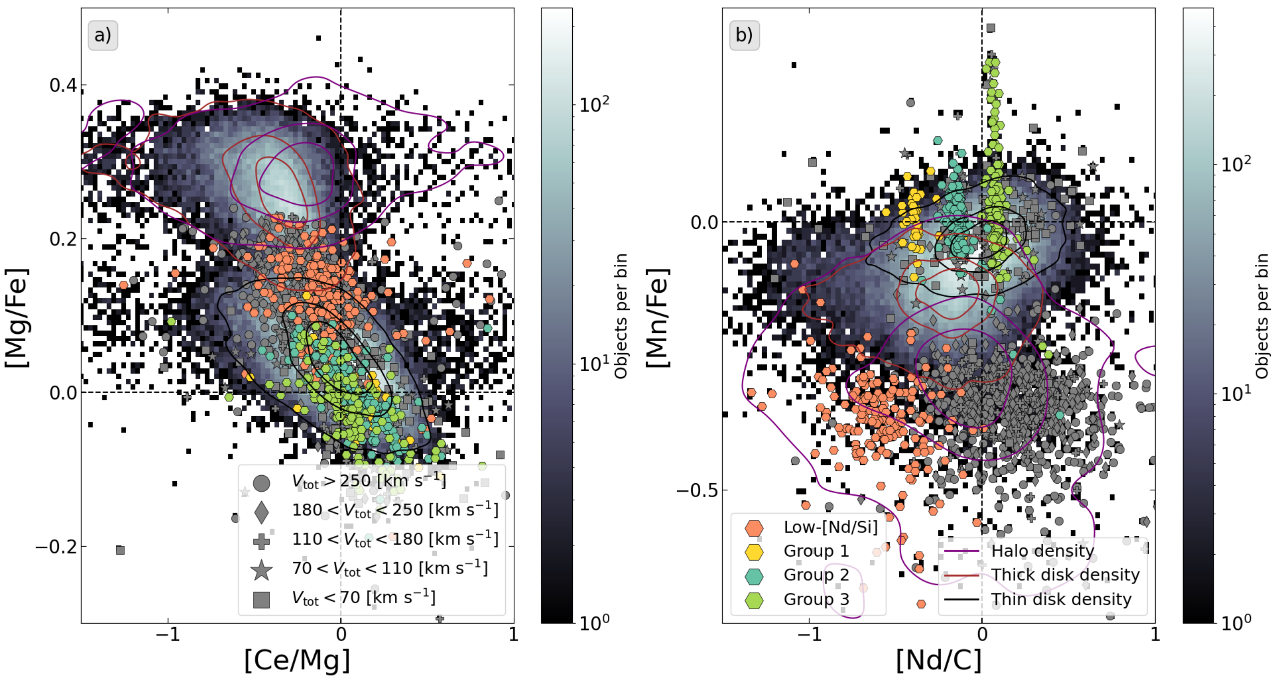

Figure 4.6: The same data as in Fig. 4.3 in the planes a) [Ce/Mg]-[Mg/Fe], and b) [Nd/C]-[Mn/Fe]. The legends applies to both figures. The dashed line indicate the solar abundance.

[Mn/Fe] compared to the other two groups.

4.2 Statistical significance

A two-sided Kolmogorov-Smirnov test (KS-test) is preformed when comparing the underlying distribution of two samples. This will be applied by comparing the low-[Nd/Si] group to the high velocity stars of the sample and the three low-[Ti/Mn] groups to the thin disk sample. This test is done to understand if the groups have independent abundance distributions or if they are simply outliers that follow an underlying distribution. Thus it can reveal if there is a statistical significance to the isolated groups, i.e. that they may be accreted stars. The probability of the group being of the same distribution as the sample is represented by a p-value, where a p-value of < 0.05 is considered significant and likely follows its own distribution. While this test does not definitively state whether a result is significant, it does indicate a probability that a sample follows a specific distribution. The KS-test can thus be used to get an indication whether an isolated group is statistically significant or seem to follow an established distribution, like the halo or the disk.

The p-values are presented in Fig. A.2 and A.3 for the abundance ratios used in the planes and some of the standard abundances. They are plotted together with the Kernel Density Estimates (KDE) for each velocity range, displaying the distribution of each grouping for the different abundances and ratios. Note that the height of the peak does not represent the count, but the density of the data at each value. The integral of each graph are equal, so a narrow range will produce a sharper peak. The combination of these will give insight into the distribution of the abundances for the sample, and could be of additional use when examining the properties of the groups.

The KDE of the low-[Nd/Si] group for the abundances and ratios is shown in Fig. A.2, where the group is compared to the high velocity range ($V_{\rm tot} > 250$ km s^{-1}) for the p-value. Looking at the KDE, the group is consistent with the high velocity ranges in ratios that does not include Nd. There is a major overlap between the group and the full sample in the two ratios including Ce. Additionally, the groups p-value is below 0.05 for most planes except for [Na/H], [Al/Fe], [Mn/Fe], [Ti/Mn], [Co/Si] and [Ce/Mg]. As for the low-[Ti/Mn] groups, Fig. A.3 exhibits that there only a single instance of a p-value indicating a similar elemental distribution as the thin disk, which is the abundance of [Ce/H]. As for the KDE of the groups, there is overlap between all three groups for all abundances except for [Nd/Si] and [Nd/C], and minor overlap for [Nd/H] and [Nd/Ce]. Group 3 tend to have a broader distribution of abundance values compared to group 1 and 2. Compared to the thin disk sample, the three groups appear to have lower abundances of both Fe-peak and α-elements.

Chapter 5

Discussion

5.1 The low-[Nd/Si] group

Since it is expected for stars to have a higher amount of neutron-capture elements if they formed in a region with slow star formation rates, one would expect halo stars to exhibit higher values of neutron-capture elements. This makes the group seen in Fig. 4.4 with a clearly lower abundance ratio stand out in the [Nd/Si]-[Ti/Mn] plane. The low-[Nd/Si] group has a low metallicity which is associated with the halo (except a few stragglers), and looking at Fig. A.2 it can be seen that this group has lower abundances of the majority of the α and the Fe-peak elements, existing in a narrower range compared to the high velocity part of the sample. The [Nd/C] ratio is notably shifted from the peak of the rest of the sample. The group also displays a higher [α/H] abundance compared to iron-peak abundances, which is in line with stars formed in an environment with gas that was not enriched by SNe Ia. The low [Nd/Si] ratio can be explained by having both a higher Si-abundance and a much lower Nd abundance compared to other sample stars. Adding that together with the low metallicity would indicate a group of older stars, which is strengthened by the high [Mg/Mn] ratio. The low [Al/Fe] ratio comes from Al being dependent on the progenitor metallicity, producing at higher rates the more free neutrons are available. The [Nd/Ce] ratio shows that this group has a much higher s-process production compared to the r-process, as the other sample stars in the same region are centred on the solar value, with the high velocity stars even reaching above that. Since r-process elements are associated with explosive events that allow for a fast rate of element production, it can be stated that these stars likely originate from a place that has not experienced such events. While the p-values for some of the ratios are above 0.05, that does not discount the other ratios that have very low p-values. So it is still likely that these stars are of an accreted origin, that are distinguished by them have much lower [Nd/H] abundances compared to the rest of the accreted sample.

Taking every detail into consideration, it is highly likely that this group is accreted, originating from somewhere that has an environment not enriched by SNe Ia nor rapid neutron-capture process, with features that strongly align with the rest of the high velocity accreted sample but stands out when the Nd abundance is investigated. The stars are not confined to a single region as seen in Fig. A.1, which could indicate it is part of a larger remnant that has settled into the Milky Way. In Fig. 4.3 the group is congregated in a way that is similar to the accreted population identified by Das et al. (2020), which could mean that this group, or some of the stars in it, belong to the GES.

5.2 The three low-[Ti/Mn] groups

In Fig. 4.3 a) the low velocity stars are similar to the accreted population seen in Feuillet et al. (2022), and could also be the low-[Al/Fe] population identified in Hawkins et al. (2015). These stars can be further separated when plotted in a plane that includes Nd, best seen in the [Nd/C]-[Mn/Fe] plane in Fig. 4.6. Group 3 extends further into higher values of [Mn/Fe], indicating a higher rate of chemical enrichment from SNe Ia compared to the other groups. In any of the planes that does not include Nd the groups are no longer distinguishable. This may be due to the observed separation being the result of enrichment caused by different r-process events, which enriched the environment to different degrees. The p-values in Fig. A.3 indicate that these groups are of a different origin than the thin disk. Thus there is a probability that these groups originate from a Galaxy that interacted with the Milky Way.

In Fig. A.1 it is clear that group 1 is closer to the solar neighbourhood, while group 2 and 3 extend into farther reaches of the Galaxy. However, all groups are primarily confined within $|z| < 2$ kpc of the plane, and with their velocity range in Fig. 4.2 some of the stars may be bound to the thin disk. The stars with higher velocities could be of the same origin but did not get captured by the thin disks dynamics. This further indicates that they belong to the same population identified in Feuillet et al. (2022). Without additional information it is difficult to say for sure if these stars are accreted and not just a part of a low-[Al/Fe] part of the thin disk. However, as discussed above there is a chance that these groups are the same as the accreted population in Feuillet et al. (2022), and using Nd helped distinguish differences in the population.

5.3 Future outlook

While a more rigorous analysis is needed to confirm that each group of stars are indeed accreted populations, it has been shown that there are chemical properties that can be highlighted in different abundance planes, specifically if Nd is included. Where the stars originally seem to be spread out in the [Al/Fe]-[Mg/Mn], introducing Nd-ratios appear to help distinguish the selected four groups of stars. Because these groups emerge with the inclusion of Nd, it could be that Nd abundance ratios will be a useful tool for identifying accreted stars. Additional information like ages, kinematics and orbits are needed to confidently say that the stars are accreted. While there is no definitive plane or ratio that determines if a star is accreted or not, these planes can help guide the selection of these stars.

Chapter 6

Conclusion

This work investigated whether new abundance planes exists that can better reveal accreted stars. To achieve this, abundances from APOGEE DR19 were used to construct abundance planes. Initially, the well known [Al/Fe]-[Mg/Mn] and [Fe/H]-[Mg/Fe] planes were used to separate the data into a sample of potential accreted stars, thus segregating the stars into regions known for hosting accreted stars. These stars were then plotted in different abundance planes and any groups that exhibited abundances that stood out from the norm were further investigated.

It was found that any planes which included Nd showed interesting groupings that stood out from the rest of the sample. One group had a significantly lower [Nd/H] abundance, indicating an origin which had not been well enriched by r-process elements compared to the other stars in the sample. In addition to that, this group also had a lower abundance of α and Fe-peak elements compared to the rest of the sample, which further indicated that these stars were born in a region which was not so chemically enriched, and could belong to the GES remnant analysed in Das et al. (2020). The three other groups all had lower [Ti/Mn] and were clearly separated in any plane including an Nd-ratio. These stars had abundances similar to a previously identified accreted population in Feuillet et al. (2022), that were found to be remnants of a previous merger bound to the disk. These results show that there are ways to further separate populations of accreted stars by investigating them in abundance planes involving Nd. Even if further analysis is required to assuredly state that these stars are of accreted origin or belong to the above mentioned established populations, this project has presented that there are abundance planes such as [Nd/Si]-[Ti/Mn] that can successfully distinguish accreted populations from each other.

Acknowledgements

I thank my supervisor Thomas Bensby and Joshua Povick for giving me valuable direction and feedback during this project. I would also like to thank my friends and family for supporting and encouraging me during this time.

Funding for the Sloan Digital Sky Survey V has been provided by the Alfred P. Sloan Foundation, the Heising-Simons Foundation, the National Science Foundation, and the Participating Institutions. SDSS acknowledges support and resources from the Center for High-Performance Computing at the University of Utah. SDSS telescopes are located at Apache Point Observatory, funded by the Astrophysical Research Consortium and operated by New Mexico State University, and at Las Campanas Observatory, operated by the Carnegie Institution for Science. The SDSS web site is www.sdss.org.

SDSS is managed by the Astrophysical Research Consortium for the Participating Institutions of the SDSS Collaboration, including the Carnegie Institution for Science, Chilean National Time Allocation Committee (CNTAC) ratified researchers, Caltech, the Gotham Participation Group, Harvard University, Heidelberg University, The Flatiron Institute, The Johns Hopkins University, L'Ecole polytechnique fédérale de Lausanne (EPFL), Leibniz-Institut für Astrophysik Potsdam (AIP), Max-Planck-Institut für Astronomie (MPIA Heidelberg), Max-Planck-Institut für Extraterrestrische Physik (MPE), Nanjing University, National Astronomical Observatories of China (NAOC), New Mexico State University, The Ohio State University, Pennsylvania State University, Smithsonian Astrophysical Observatory, Space Telescope Science Institute (STScI), the Stellar Astrophysics Participation Group, Universidad Nacional Autónoma de México, University of Arizona, University of Colorado Boulder, University of Illinois at Urbana-Champaign, University of Toronto, University of Utah, University of Virginia, Yale University, and Yunnan University.

Bibliography

Astropy Collaboration, Price-Whelan, A. M., Lim, P. L., et al. 2022, ApJ, 935, 167

Battistini, C. & Bensby, T. 2016, A&A, 586, A49

Bensby, T., Feltzing, S., Gould, A., et al. 2017, A&A, 605, A89

Bensby, T., Feltzing, S., & Oey, M. S. 2014, A&A, 562, A71

Bowen, I. S. & Vaughan, A. H. 1973, Appl. Opt., 12, 1430

Buder, S., Lind, K., Ness, M. K., et al. 2021, MNRAS, 510, 2407

Buder, S., Mijnarends, L., & Buck, T. 2024, MNRAS, 532, 1010

Das, P., Hawkins, K., & Jofré, P. 2020, MNRAS, 493, 5195

Feuillet, D. K., Feltzing, S., Sahlholdt, C., & Bensby, T. 2022, ApJ, 934, 21

García Pérez, A. E., Allende Prieto, C., Holtzman, J. A., et al. 2016, AJ, 151, 144

Gray, D. F. 2005, The Observation and Analysis of Stellar Photospheres (Cambridge University Press)

Gunn, J. E., Siegmund, W. A., Mannery, E. J., et al. 2006, AJ, 131, 2332

Hawkins, K., Jofré, P., Masseron, T., & Gilmore, G. 2015, MNRAS, 453, 758

Helmi, A. 2020, ARA&A, 58, 205

Horta, D., Schiavon, R. P., Mackereth, J. T., et al. 2021, MNRAS, 500, 1385

Kawata, D., Grand, R. J. J., Hunt, J. A. S., & Ciucă, I. 2026, in Encyclopedia of Astrophysics, Volume 4, Vol. 4, 38–60

Kobayashi, C. 2026, in Encyclopedia of Astrophysics, Volume 2, Vol. 2, 744–777

Kobayashi, C., Karakas, A. I., & Lugaro, M. 2020, ApJ, 900, 179

Kollmeier, J. A., Rix, H.-W., Aerts, C., et al. 2026, AJ, 171, 52

Majewski, S. R., Schiavon, R. P., Frinchaboy, P. M., et al. 2017, AJ, 154, 94

Matteucci, F., Grisoni, V., Spitoni, E., et al. 2019, MNRAS, 487, 5363

Mészáros, S., Jofré, P., Johnson, J. A., et al. 2025, AJ, 170, 96

Necib, L., Ostdiek, B., Lisanti, M., et al. 2020, Nature Astronomy, 4, 1078

Nissen, P. E. & Schuster, W. J. 2010, A&A, 511, L10

Queiroz, A. B. A., Anders, F., Chiappini, C., et al. 2023, A&A, 673, A155

Queiroz, A. B. A., Anders, F., Chiappini, C., et al. 2020, A&A, 638, A76

SDSS Collaboration, Adamane Pallathadka, G., Aghakhanloo, M., et al. 2025, arXiv e-prints, arXiv:2507.07093

Wilson, J. C., Hearty, F. R., Skrutskie, M. F., et al. 2019, PASP, 131, 055001

Zoccali, M. & Valenti, E. 2026, in Encyclopedia of Astrophysics, Volume 4, Vol. 4, 19–37

Appendix A

Additional figures

A.1 Galactic Position

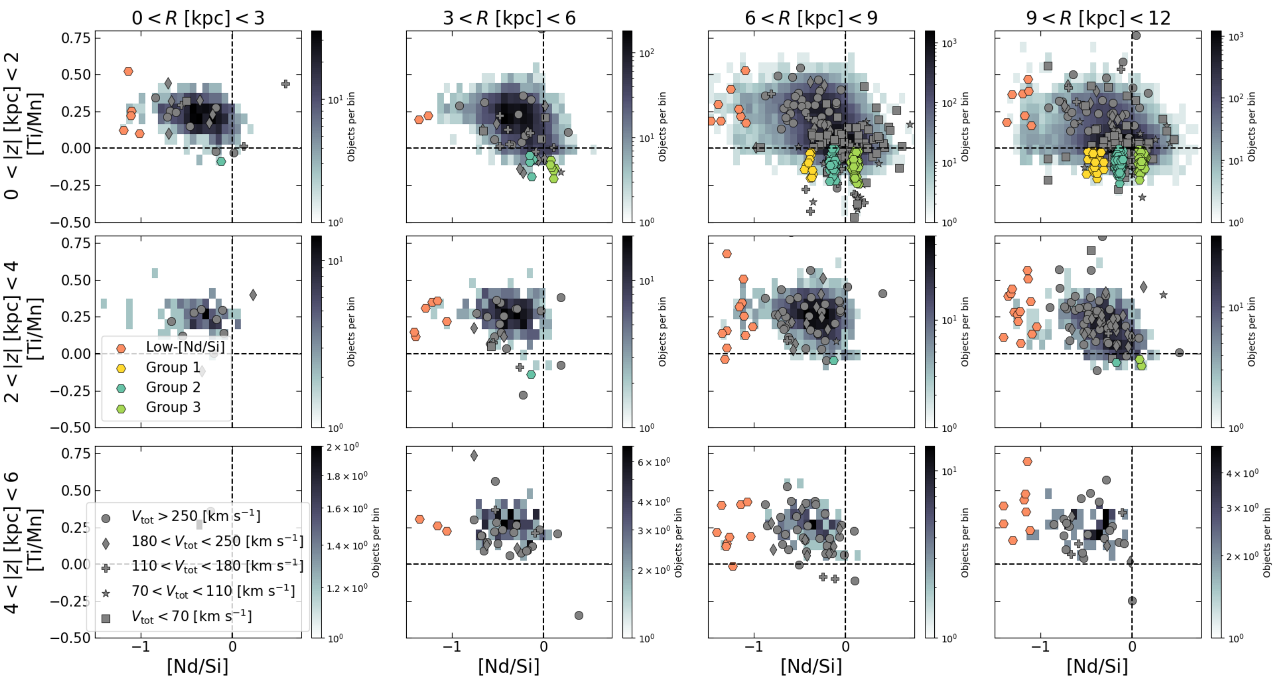

Figure A.1: The isolated groups varied by distance R from the Galactic centre and the absolute distance from the plane $|z|$. The colours and symbols are the same as in Fig. 4.3.

A.2 Low-[Nd/Si] group

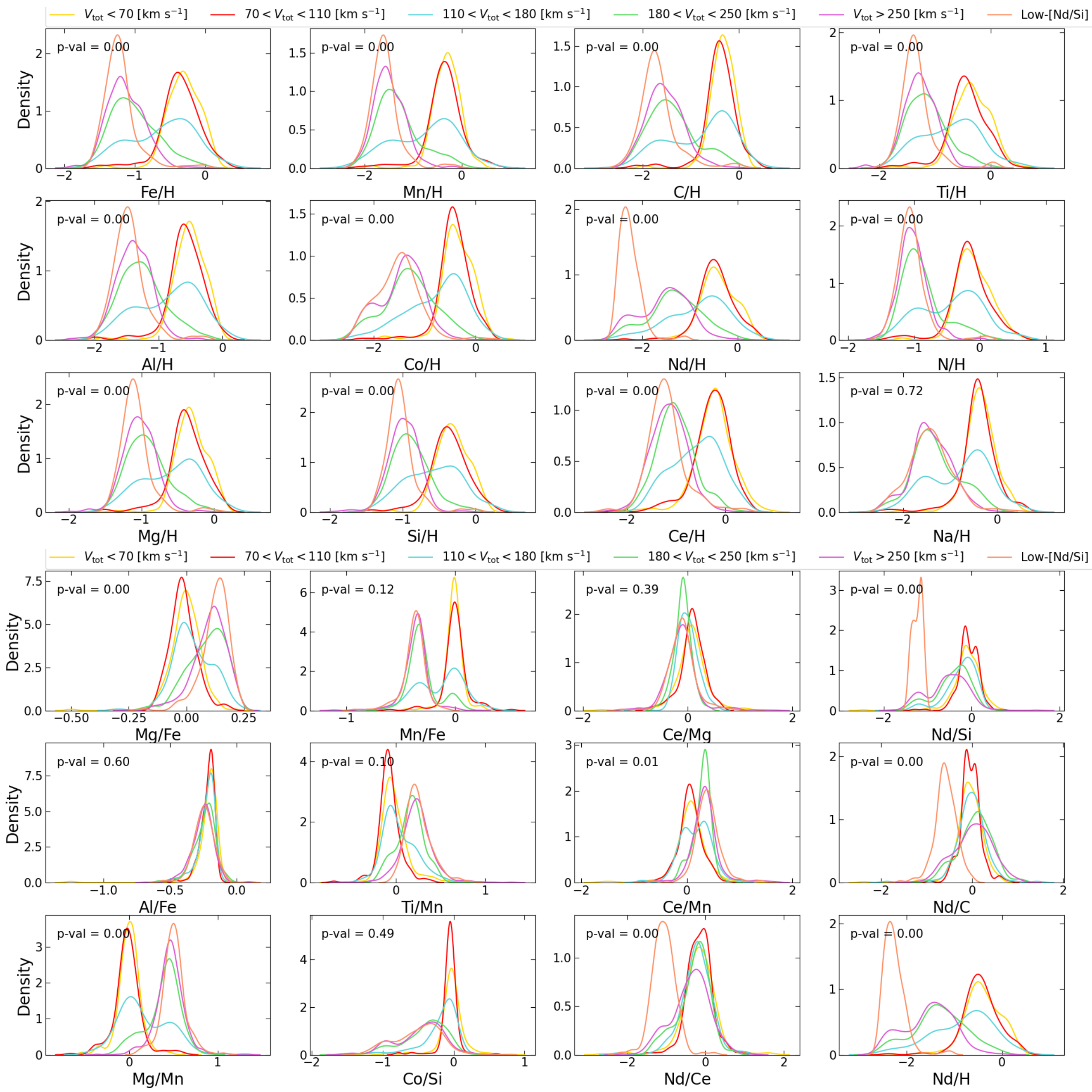

Figure A.2: Kernel density estimates for some of the abundances included in APOGEE, displaying the full sample with velocity divisions and the isolated low-[Nd/Si] group. The p-value is taken between the low [Nd/Si] group and the high velocity group due to the observed overlap.

A.3 Low-[Ti/Mn] Groups

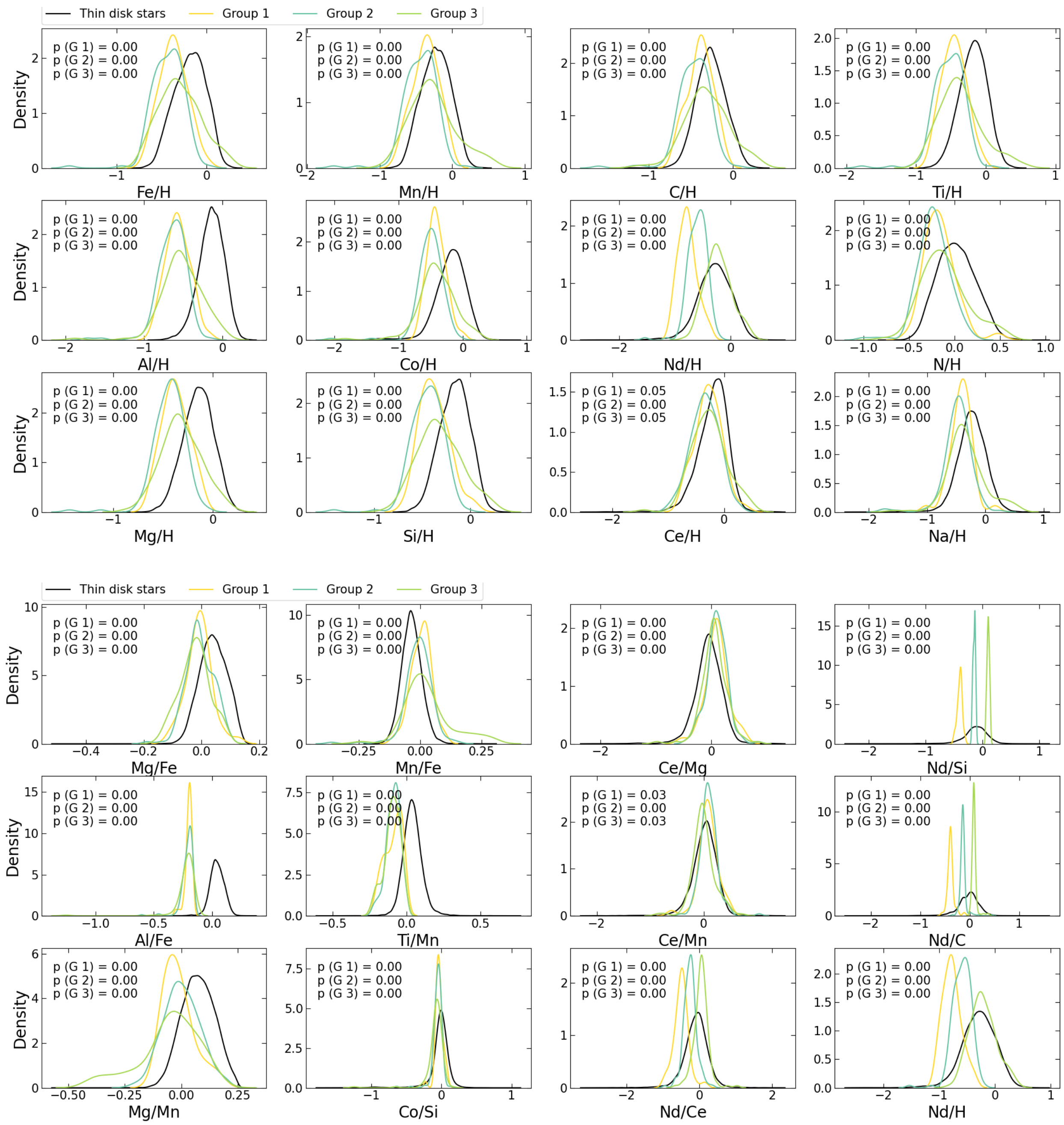

Figure A.3: Kernel density estimates for some of the abundances included in APOGEE, displaying the three low-[Ti/Mn] groups and the thin disk sample defined in Table 3.1. The p-value is taken between the specified group (G 1-3) and the thin disk sample to gain insight into whether they could be accreted or formed in-situ.